Theoretical Chemistry Accounts (2019) 138:113
https://doi.org/10.1007/s00214-019-2502-6

REGULAR ARTICLE

A density functional theory study on complexation processes and intermolecular interactions of triptycene-derived oxacalixarenes

Zishang Jia[1] · Hongdi Pang[1] · Hui Li[1] · Xueye Wang[1]

Received: 2 April 2019 / Accepted: 28 August 2019 / Published online: 3 September 2019

Abstract
Triptycene-derived oxacalixarenes (TP) exhibit two different conformations: *cis*-isomer (TPA) and *trans*-isomer (TPB). The geometries structures were optimized by the density functional theory (DFT) based on ωB97XD and B3LYP-D3 functionals. The oxacalixarenes favor the inclusion complex through noncovalent interactions, such as hydrogen bonding, $\pi\cdots\pi$ stacking, and C–H$\cdots\pi$ interactions. The formation of a inclusion complex is spontaneous and thermodynamically favorable. The calculated ^{1}H nuclear magnetic resonance (^{1}HNMR) spectrum of MV^{2+}@TPA (MV^{2+}: methyl viologen cation) showed the chemical shifts of its protons have changed upon complexation. The frontier molecular orbitals and the energy of band gap were constructed and analyzed. The interaction between host and guest was investigated and characterized by the molecular electrostatic potential (MESP), vibration frequency, the natural bond orbital (NBO), and quantum theory of atoms in molecules (AIM) methods. And also the reduced density gradient (RDG) isosurface map and scatter diagram reflected the location and intensity of the noncovalent interactions.

Keywords Density functional theory · Host–guest · Noncovalent interactions · Oxacalixarene · Triptycene

1 Introduction

Supramolecular chemistry is a new discipline. It is based on the development of macrocyclic ligands such as crown ethers and cryptands, as well as the study of molecular self-assembly and the development of organic semiconductors or conductors. In recent years, supramolecular chemistry has developed rapidly in many fields, like molecular self-assembly, molecular recognition, host–guest chemistry, and dynamic covalent chemistry [1–4]. In the field of supramolecular chemistry, the development of the host–guest system plays an important role, especially in host recognition and the guest complexation.

The host–guest system refers to a chemical system in which a host molecule and one or more guest molecules interact through nonvalence bonds in a controlled manner. The host is usually an electron-rich molecule that acts as an electron donor, such as a base, an anion, a nucleophile, and so on. The guest is an electron-deficient molecule that acts as an electron acceptor, such as an acid, a cation, an electrophile, and so on. Normally, the formation of a host–guest system involves more than one type of noncovalent interaction, like hydrophobic association, hydrogen bonding, electrostatic interactions, metal coordination, van der Waals forces, and π–π stacking interactions. So far the macrocyclic compounds for mechanically interlocking molecules, including crown ethers [5–7], cyclophanes [8–10], and cyclodextrins [11–14], have been reported. The emergence of newer macrocyclic hosts has accelerated the expansion of this field with their potential applications in interdisciplinary areas including catalysis [15], molecular machines [16], and supramolecular polymers [17]. Based on these, calixarene, as the third generation of host molecules after crown ether and cyclodextrin, become more and more popular in various areas. Similar to the macrocyclic host compounds like crown ethers and cyclodextrins, calixarene is recognized by molecules of synthetic receptors and selectively binds with the guest (ion or neutral molecule) to form a supramolecular system. Calixarene, easy to synthesize and to chemically

✉ Xueye Wang
wxueye@xtu.edu.cn

[1] Key Laboratory for Green Organic Synthesis and Application of Hunan Province, Key Laboratory of Environmentally Friendly Chemistry and Applications of Ministry of Education, College of Chemistry, Xiangtan University, Xiangtan 411105, Hunan, People's Republic of China

modify, has special structural properties, which creates a good platform for the development of molecular and ionic complexing agents [18, 19].

At present, a new type of calixarene is constructed by introducing a heteroatom to replace the methylene group or introducing another aromatic ring system to replace the phenol unit. With the consideration of small cavities of some heteroatom calixarene, triptycene derivatives as nucleophilic substrates have been used to synthesize heteroatom calixarene with larger cavities [20, 21]. Yang et al. also introduced a sulfuryl group and an amide group into the triptycene structure [22] and found that the intramolecular and intermolecular amide–amide hydrogen bonds, the folded structure of the sulfothio group, and the π–π interactions from aromatic hydrocarbons on the opposite side of triptycene together affect the structure of the assembly. The triptycene-calix[6]arene [23] and the oxacalix[6]arene [24] form an organic tubular structure and a porous advanced supramolecular assembly in a solid state. Triptycene-derived oxacalixarene and tetraoxacalix[2]-triptycene[2]naphthyridine showed highly efficient complexation abilities toward the fullerenes C60 and C70 [25]. In addition, Chen et al. used triptycene-derived oxacalixarenes as wheel to synthesize [2]rotaxanes and proposed a scheme for identifying differences in different guest molecules by ion regulation or acid–base regulation [26].

The present work precisely focuses on supramolecular interactions accompanying the host–guest complexation, in particular the selectivity of triptycene-derived oxacalixarenes to the paraquat derivatives. Here, a paraquat derivative consisting of methyl viologen cation (*N*, *N*-dialkyl, 4, 4-bipyridinium) (MV^{2+}) and PF_6^- is selected for the guest recognition. The PF_6^- of the guest molecule does not involve in the noncovalent interactions. Therefore, this work focuses on the selection and identification of cations by the host molecules. The density functional theory (DFT) was used to optimize and analyze the structures. The noncovalent interactions (NCI) [27] methods and the quantum theory of atoms in molecules (AIM) were used to analyze the weak interaction, and a summary of noncovalent interactions of such host–guest binding has been proposed.

2 Computational details

In this work, all the presented calculations have been performed with the Gaussian 09 software package [28]. The density functionals of ωB97XD [29] and B3LYP-D3 [30, 31] were employed for this system. The two functionals, introducing both the long-range corrected and DFT-D schemes, are considered to provide reasonably accurate description of the noncovalent interactions. The geometric configurations were optimized at 6-311 + G(d, p) level. The interaction energies of the host and the guest molecules were carried out applying ωB97XD and B3LYP-D3 functionals, which provided the correction of the total electronic energy besides distinguishing intermolecular weak interaction. And the interaction energies were corrected using the basis set superposition error (BSSE) method [32] to make the results accurate. The initial structures were obtained by using the GaussView 5.0.8 program [33]. All of the optimized structures were at the same basis set and confirmed without imaginary frequency.

The energy of the frontier molecular orbital was studied to estimate the stability of structures. The molecule is more stable with greater HOMO–LUMO energy gap. The molecular electrostatic potential (MESP) [34] can be used to characterize the charge distribution within the cavity of the host molecule. The nuclear magnetic resonance (NMR) spectra were investigated by the gauge-independent atomic orbital (GIAO) method [35], with TMS employed as a reference [36]. In order to simulate the solvent environment, the NMR calculation was carried out in solvent phase adopting a polarized continuum model (PCM) [37, 38] using $CDCl_3/CD_3CN$(2:1) solvent [26] with dielectric constants of 4.71 and 35.69, respectively. Infrared spectra were used to analyze the vibration frequencies and displacements of the characteristic peaks before and after the complexation. Additionally, to estimate the strength of hydrogen bond, C–H$\cdots\pi$ and $\pi\cdots\pi$ stacking within the complex, the natural bond orbital (NBO) analysis [39] is calculated for all the optimized structures. Besides, a visual study of weak interaction was performed by calculating the reduced density gradient (RDG) and using the visual molecular dynamics (VMD) package [40]. The method applies a reduced density gradient at various points in space function and calculates the value of $\mathrm{sign}(\lambda 2(r))\rho(r)$ function. The RDG isosurface map visually reveals the molecular regions associated with weak interactions. Its formula is defined as follows:

$$s = \frac{1}{2\left(3\pi^2\right)^{1/3}} \frac{|\nabla\rho(r)|}{\rho(r)^{4/3}}$$

where $\rho(r)$ is the critical point of weak interaction in molecular theory. There is a positive correlation between the value and the strength of the bond. The $\mathrm{sign}(\lambda 2(r))$ function is the sign of the second largest eigenvalue $\lambda 2$ of the electron density Hessian matrix, which can be used to reflect the type of the bond. Further, the topological analysis of atoms in molecules (AIM) [41] has been calculated via Multiwfn program [42, 43].

3 Results and discussions

3.1 Structure and geometry

Due to the naphthalene's flipping, triptycene-derived oxacalixarenes are divided into two conformations: TPA and TPB, which are diastereomers of each other. The conformations showed not only a large cavity but also a fixed conformation in solution and the solid state at room temperature [26]. The structures composed of triptycene subunits and bridged naphthyridine groups (as seen in Fig. 1), TPA adopts a *cis*-isomer with a boat-like 1,3-alternate conformation, and TPB adopts a *trans*-isomer with a curved boat-like conformation. The symmetrical structures can be clearly seen in Fig. 1, and the formed cavity can help to better identify the guest molecules.

To understand the complexation process, the guest molecules were encapsulated into the body cavity (refer to Fig. 2). It can be considered as a reaction: Host molecules bind with the guest to form complexes. Triptycene-derived oxacalixarenes (TP) complex with the methyl viologen (MV^{2+}), called MV^{2+}@TP. When the linear axis MV^{2+} molecule passes through the host cavity, the guest is encapsulated in the large cavity due to the recognition of the host molecule. Selected structural parameters of the guest and the complexes are summarized in Table 1. The bond length variation of the guest MV^{2+} in the host cavity is small, and the variation range is within 0.003 Å. It denotes that the bond length is nearly insensitive to the complexation. The reduction in the bond angle of N76-C66-N75 after complexation indicates that the size of the cavity is contracting. As may be noticed, the two pyridine rings in MV^{2+}@TPA and MV^{2+}@TPB tend to attain planarity (deviation up to 27.18° and 22.99°, respectively). This may be ascribed to the asymmetric environment provided by the large ring. It is consistent with the inferences drawn from the work of Chen [26]. In fact, the nitrogen atoms N98 and N107 on the pyridine are not in the same plane, which indicates that the lone pair of nitrogen atom is not fully involved in π-conjugation. The addition of MV^{2+} within the host molecule brings the contraction of its cavity, which illustrates the interaction between the molecules.

3.2 Interaction energies and thermodynamic properties

In order to evaluate the stability of the complex (MV^{2+}@TPA and MV^{2+}@TPB) between the host and guest systems, the interaction energy ΔE_{CP} is calculated using B3LYP-D3 and ωB97XD functionals at 6-311 + G(d, p) level. The interaction energy is equal to the difference between the energy of the host–guest complex and the sum of the energy of the host and the guest. Besides, the basis set superposition error (BSSE) corrections are also taken into account to obtain

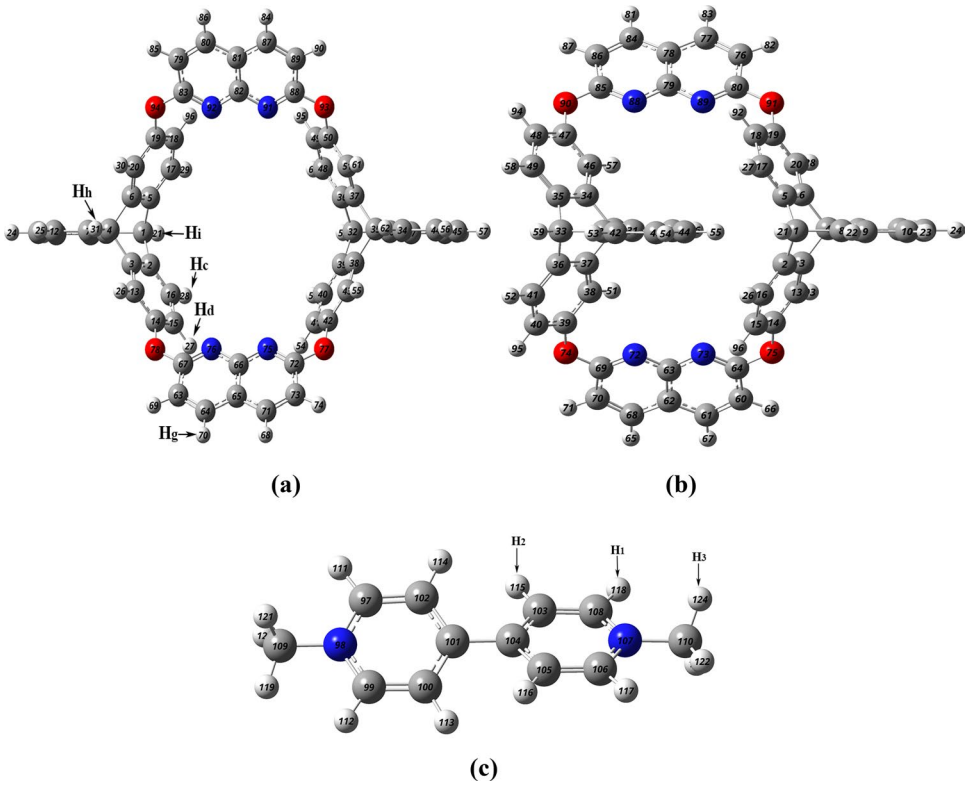

Fig. 1 Optimized structure of **a** TPA molecule, **b** TPB molecule and **c** guest molecule. The red and blue colors are for oxygen atoms, nitrogen atoms, respectively

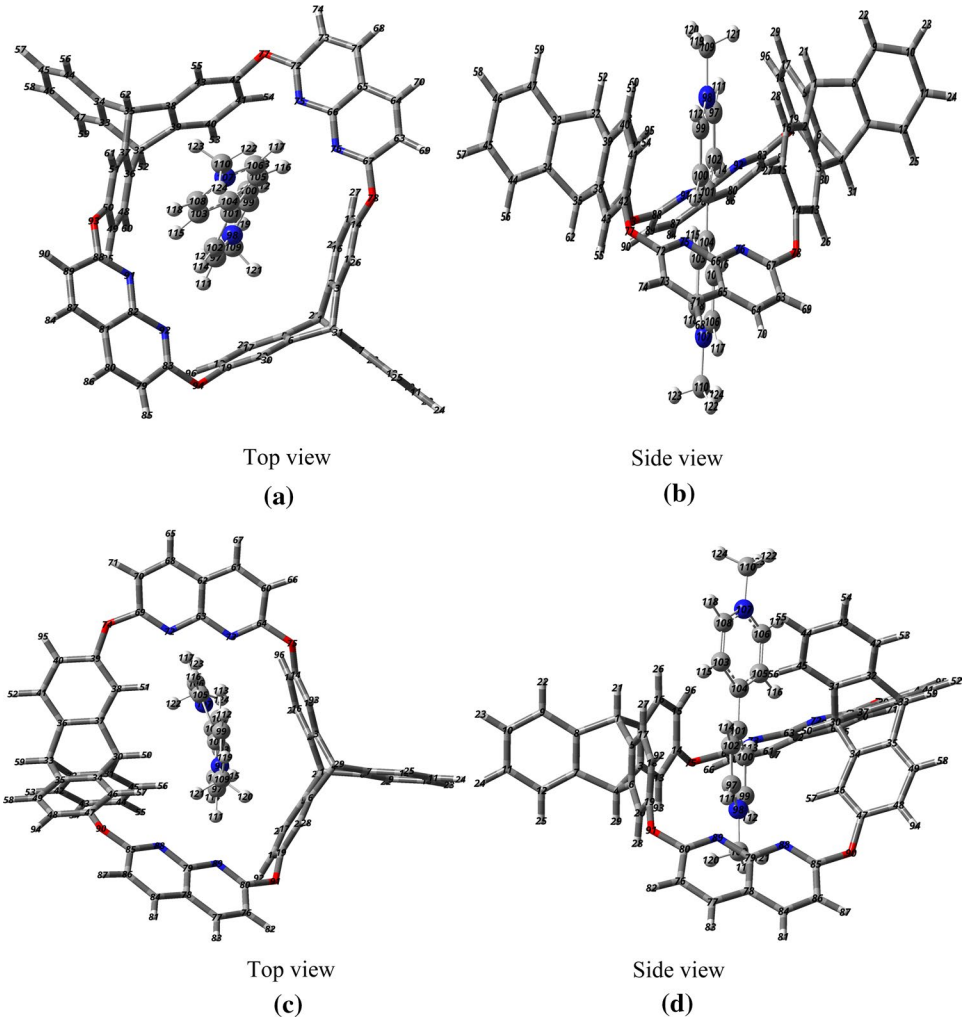

Fig. 2 **a** Top view and **b** side view of optimized MV^{2+}@TPA complexes, **c** top view, and **d** side view of optimized MV^{2+}@TPB complexes

Table 1 Selected geometrical parameters (bond distances in Å and angles in °) in the guest, host, and their complexes

	MV^{2+}	TPA	TPB	MV^{2+}@TPA	MV^{2+}@TPB
R(C103–C104)	1.399	–	–	1.401	1.400
R(C101–C104)	1.479	–	–	1.476	1.477
R(C108–N107)	1.350	–	–	1.352	1.352
R(C103–H115)	1.080	–	–	1.083	1.086
R(C67=N76)	–	1.306	1.305	1.309	1.305
R(C88–O93)	–	1.361	1.361	1.361	1.361
θ(N76–C66–N75)	–	116.3	116.4	115.8	115.8
θ(C108–N107–C103)	120.7	–	–	120.6	120.9
θ(C102–C101–C104–C103)	39.25	–	–	27.17	22.99
θ(C103–C108–N107–N110)	178.6	–	–	179.9	177.7

more accurate interaction energy. The interaction energy is obtained using the counterpoise method for the host–guest complexes. All the ΔE is negative, and the larger absolute value of ΔE means that the more stable system is going to be. The interaction energies and the thermodynamic properties are calculated as illustrated in Table 2. The ΔE_{CP} obtained at ωB97XD/6-311 + G(d, p) level is very close to that of B3LYP-D3/6-311 + G(d, p) level, and the relative orders of the complexes at above two levels of theory are completely the same. Therefore, the relative stabilities of the complexes could be reliable. The two functionals are both considered to provide reasonably accurate description of the noncovalent interactions. However, B3LYP-D3 functional has advantages on both time and cost of calculation

Table 2 Interaction energy (ΔE, kcal/mol), BSSE-corrected interaction energy (ΔE_{CP}, kcal/mol), reaction free energy (ΔG, kcal/mol), reaction enthalpy (ΔH, kcal/mol) for the complexes

System	ΔE (kcal/mol)		ΔE_{CP} (kcal/mol)		ΔG (kcal/mol)	ΔH (kcal/mol)
	B3LYP-D3	ωB97XD	B3LYP-D3	ωB97XD		
MV^{2+}@TPA	− 33.45	− 34.58	− 28.73	− 29.55	− 211.13	− 234.44
MV^{2+}@TPB	− 27.48	− 27.17	− 23.09	− 22.45	− 217.74	− 233.74

compared to ωB97XD functional; it seems that B3LYP-D3 is more suitable for this calculation for us. By comparison, the BSSE-corrected interaction energy (ΔE_{CP}) of MV^{2+}@TPA complex (− 28.73 kcal/mol) has a larger negative value compared to that of MV^{2+}@TPB complex (− 23.09 kcal/mol), which means the MV^{2+} forms a more stable complex with TPA compared to the TPB. Besides, the thermodynamic properties under the B3LYP-D3 functional are also listed in Table 2. The values of ΔH and ΔG for the system are negative, which indicates the reaction is more likely to happen. The reaction enthalpy (ΔH) suggests the process is exothermic in nature, and the negative reaction free energy (ΔG) implies the thermodynamic spontaneity of the process. The results showed that the properties of MV^{2+}@TPA and MV^{2+}@TPB complexes were approximately the same, and MV^{2+}@TPA was slightly stable. Thus, the results presented in the following calculation and analysis will be primarily devoted to MV^{2+}@TPA system.

3.3 Molecular electrostatic potential analysis (MESP)

Molecular electrostatic potential (MESP) is a description of the interaction between nuclear charge and electrons. In a certain area, as the electrostatic potential on the surface of the molecule becomes more negative, the molecular is more susceptible to be attacked by positively charged electrophiles. Conversely, when the electrostatic potential becomes more positive, the molecular is more susceptible to be attacked by negatively charged nucleophile. Since the nucleus and electron coexist in the molecular system, the positively charged nucleus and the negatively charged electron will affect the electrostatic potential of the molecule. Therefore, there is an electrostatic field everywhere in the space. The distribution diagram of MESP can visually show which areas are positively charged or negatively charged. Generally, red implies negative potential regions and blue signifies positive electrostatic potential. In this paper, the electrostatic potentials on the surface of TPA and MV^{2+} are shown by the color isosurface in Fig. 3. In terms of TPA molecule, the negative-valued MESP is centered on the nitrogen and oxygen atoms, which presents a red area. It is attributed to the lone pair of heteroatoms around the naphthyridine and the delocalized π-electron cloud. It can be speculated that TPA molecule is electron-rich and capable of accommodating methyl viologen cation MV^{2+} in its cavity. It can also be observed that the aromatic ring shows a pale-yellow color and the periphery of the cavity shows a light-blue color. The positive electrostatic potential distribution appears dark-blue on the surface of the entire MV^{2+} molecule. The electron-rich nature of the TPA cavity complements the electron-deficient properties exhibited by MV^{2+}, which form a stable host-guest system through the electrostatic interactions.

3.4 Molecular orbitals (HOMO and LUMO)

The highest occupied molecular orbital (HOMO) and the lowest empty molecular orbital (LUMO) are popular quantum mechanical descriptors; especially, the HOMO–LUMO energy gap is an important parameter to study the stability of molecular. The molecular orbital diagrams of ground

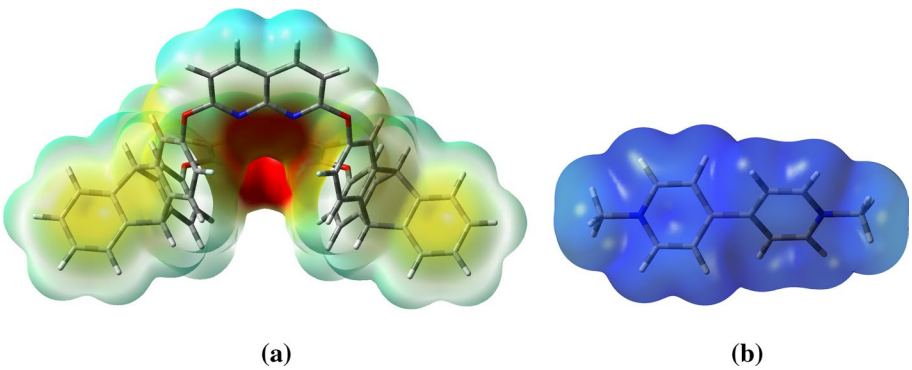

(a) (b)

Fig. 3 Electrostatic potentials on the surface of **a** TPA and **b** MV^{2+}, isosurface is 0.01 a.u. and the range is − 0.06 a.u. to 0.06 a.u. Red and blue colors indicate negative and positive regions, respectively

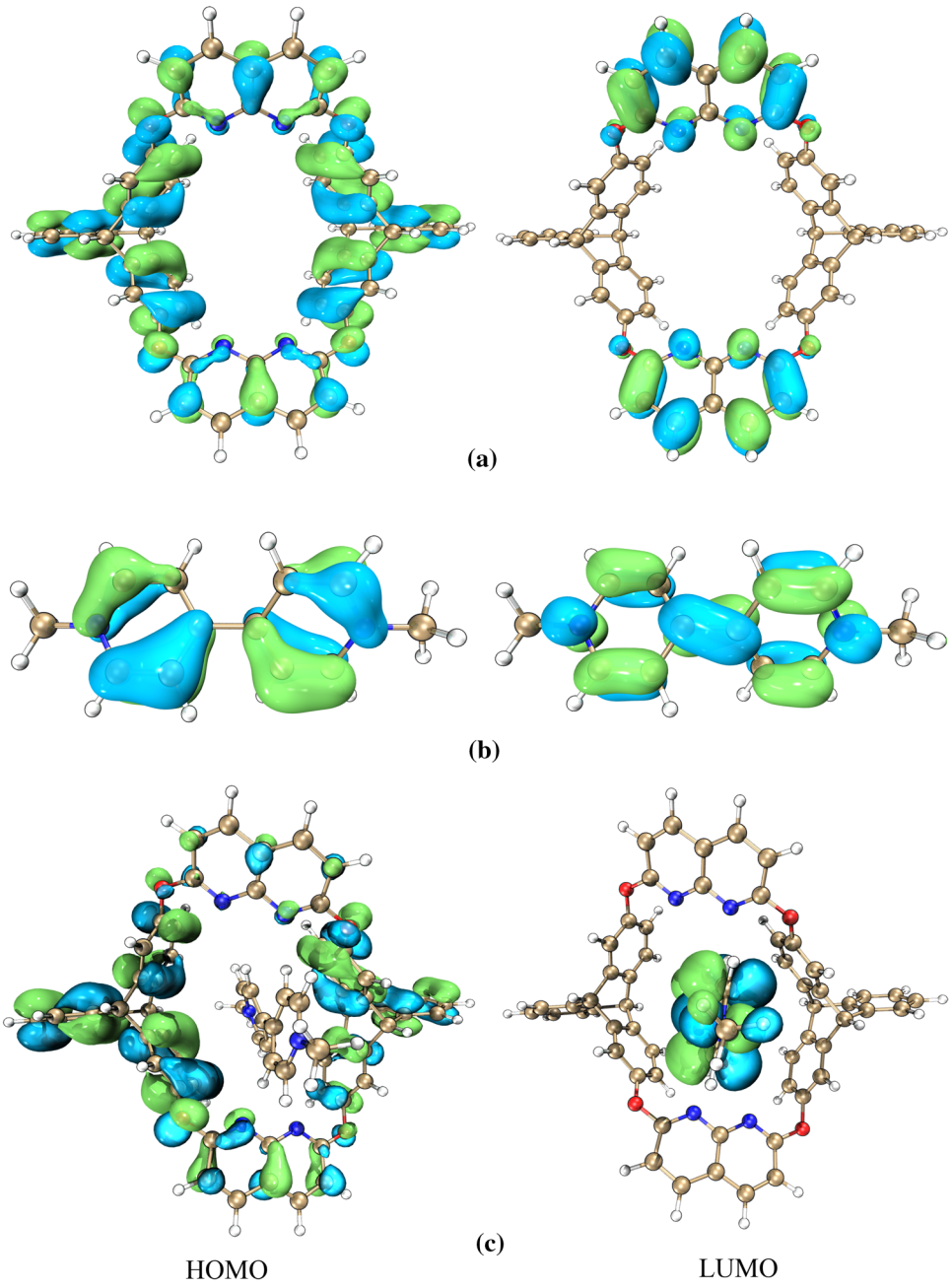

Fig. 4 The frontier molecular orbital in **a** TPA, **b** MV^{2+}, and **c** MV^{2+}@TPA

state molecules are shown in Fig. 4. The HOMO of the TPA host mainly distributed around the benzene ring of the triptycene. It indicates that the benzene ring has a strong ability to donate electrons. The LUMO has been mainly localized near the naphthalene moiety, which shows the naphthalene is easier to accept electrons. The penetration of the guest within a host cavity revealed that the HOMO was located on the benzene of triptycene whereas the LUMO located on the MV^{2+} guest. This shows the transition from HOMO to LUMO which causes the charge to be transferred from the host to the guest molecule. Furthermore, the calculated energies of the molecular orbital are presented in Table 3.

Table 3 Frontier molecular orbital energy parameter in the free TPA, TPB, MV^{2+}, and their complexes

Species	MV^{2+}	TPA	TPB	MV^{2+}@TPA	MV^{2+}@TPB
E_{HOMO} (eV)	−9.35	−5.72	−5.83	−6.39	−6.30
E_{LUMO} (eV)	−4.10	−1.69	−1.82	−3.92	−4.06
$\Delta E_{LUMO-HOMO}$ (eV)	5.25	4.03	4.01	2.47	2.24

Concerning the value of the energy gap $\Delta E_{\text{LUMO-HOMO}}$, higher values of $\Delta E_{\text{LUMO–HOMO}}$ will provide lower reactivity to a chemical species. Lower values of the energy difference will indicate the higher reactivity of the molecules, because the energy to remove an electron from the last occupied orbital to the first unoccupied orbital will be low. In this system, the calculated HOMO energy of MV^{2+}@TPA is −6.39 eV and the LUMO energy is −3.92 eV; the energy difference between HOMO and LUMO is 2.47 eV. It is larger than MV^{2+}@TPB (2.24 eV). This signifies that the stability of the MV^{2+} binding with TPA is higher, consistent with the previous analysis.

3.5 NMR studies

The molecular structure of the host and guest was optimized at the DFT-D3 (B3LYP)/6-311G (2d, p) level using the GIAO method. The GIAO-derived δH values of the host, guest, and their complexes were computed with the use of $CDCl_3/CD_3CN$ (2:1) as solvent and the tetramethylsilane (TMS) as internal standard at room temperature. In order to compare the ^{1}HNMR chemical shifts of different oxidation states of the methyl viologen guest in the TPA molecule, the MV^0 guest molecule has been introduced. The computed δH values of the host, guest, and their complexes are presented in Table 4. The two protons on the benzene ring of triptycene are recorded as H_c, H_d, the bridgehead protons recorded as H_h and H_i, and the proton on 1,8-naphthyridine recorded as H_g. The methyl viologen protons are broadly classified as pyridine protons (H_1 and H_2) and methylene protons (H_3). Table 4 shows that when the free state TPA forms into the complex, the chemical shifts of H_c, H_d, H_h, and H_i on the macrocycle all move to the upfield ($\Delta\delta < 0$). It reveals that the benzene ring of triptycene accumulates more negative charges and the shielding effect becomes larger after the guest was encapsulated. However, the chemical shift of proton H_g moves to the downfield ($\Delta\delta = 0.26$), which denotes the density of electron clouds around 1,8-naphthyridine decreases. When the nitrogen atom on the naphthyridine forms a C–H···N hydrogen bond with the guest molecule, the electron cloud density around the hydrogen nucleus decreases, causing the chemical shift to move to the downfield. It follows the same order as observed in the experimental ^{1}HNMR spectra [26]. The chemical shifts of protons H_1, H_2, H_3 on the guest MV^{2+} are reduced compared to the MV^{2+}@TPA. The hierarchy of the calculated δH values turns out to be $H_1 > H_2 > H_3$ for the isolated MV^{2+}. With the chemical shift moving to the upfield, the electron cloud density becomes higher, and the shielding effect becomes larger. By comparing the values of H_1, H_2, H_3 in the oxidized state MV^{2+} with that of reduced state MV^0, it showed that H_1 (8.82 ppm), H_1 (8.77 ppm), H_3 (4.52 ppm) in MV^{2+} are more deshielded than those of MV^0. The different oxidation states of the methyl viologen make the proton on the pyridine ring different, resulting in different chemical shifts. In the process of inclusion, it can be inferred from the proton exhibiting upfield signal that the MV^0 and MV^{2+} guests are completely embedded in the TPA cavity. The guest molecule is encapsulated in the host cavity, which is consistent with the previous optimization structure analysis.

Table 4 ^{1}HNMR chemical shifts (ppm) of free TPA, MV^{2+}, MV^0, and their complexes

δ_H	TPA	MV^{2+}	MV^0	MV^{2+}@TPA	MV^0@TPA
H_c	7.69	–	–	6.92	7.65
H_d	7.54	–	–	7.01	7.07
H_g	8.29	–	–	8.56	8.45
H_h	5.51	–	–	5.25	5.00
H_i	5.39	–	–	5.05	5.13
H_1	–	8.82	6.58	8.32	5.78
H_2	–	8.77	5.43	8.56	5.13
H_3	–	4.52	2.52	4.38	2.41

3.6 Vibrational frequency and NBO analysis

As the guest molecule encapsulates into the structure of the host molecule, its vibration frequency changes, reflected in the infrared spectrum as shown in Fig. 5. The isolated guest molecule MV^{2+} has a weak peak at 3238 cm^{-1}, originated from C–H on bipyridine. After MV^{2+} complexed with the host, the vibration shifted from 3238 to 3180 cm^{-1} (redshift 58 cm^{-1}). The direction of C–H stretching vibration is toward the nitrogen atom on naphthyridine. It is conducive to promote the formation of C–H···N hydrogen bond in the host–guest system. In addition, the peak at 982 cm^{-1} was attributed to the stretching mode of the C–O bond, and a small blueshift of 3 cm

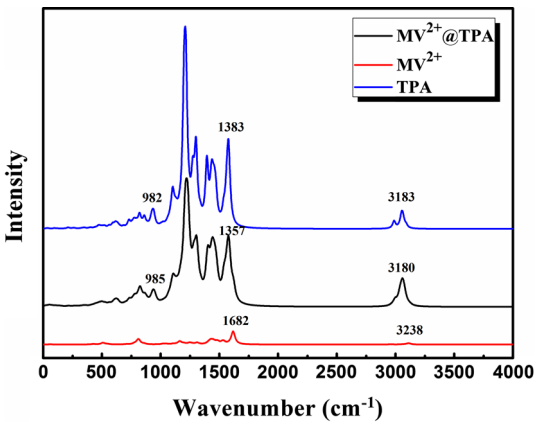

Fig. 5 Vibrational spectra of MV^{2+}, TPA, and their complexes MV^{2+}@TPA

occurred after the complexation. A 26 cm^{-1} redshift of the C=N stretching mode (1357 cm^{-1}) is also observable in the IR spectra, verifying the existence of weak intermolecular interactions (e.g., C–H···π interaction). The redshift or blueshift of the vibration frequency indicates a certain change in the structure of the host and guest before and after complexation. This may be due to the flipping of naphthyridine, which changes the structure and forms the intermolecular interaction between the host and the guest. It is consistent with the previous structural analysis. Thus, the vibration frequency and intensity patterns provide a fingerprint for typifying the noncovalent interactions of the host–guest system.

In order to further investigate the interaction between atoms in the above complexation process, NBO analysis was performed utilizing B3LYP-D3/6-311 + G(d, p) level of theory. The orbital bond and charge transfer have been analyzed. When the orbital symmetry of similar energy levels is matched, the charge transfer can occur, and the delocalization effect of the charge is generated; the corresponding system energy will also decrease. The stabilization energy $E^{(2)}$ associated with the delocalization from donor (i) to acceptor (j) can be written as follows:

$$E^{(2)} = \Delta E_{ij} = q_i \frac{F^2_{(i,j)}}{\varepsilon_j - \varepsilon_i}$$

where q_i is the donor orbit occupancy, ε_j and ε_i are the orbital energies, and $F_{(i,j)}$ is the off-diagonal NBO fock matrix element. And the interacting stabilization energy was estimated by the second-order perturbation theory. As the $E^{(2)}$ is larger, the interaction becomes stronger and the corresponding system will be more stable. The details of NBO analyses for MV^{2+}@TPA are presented in Table 5; it displays the interaction orbitals and its interaction strength.

The NBO calculated results confirm that the charge transfer is between the orbital of the host and guest molecule. With more charge transfer, the interaction between the host and the guest becomes more obvious. As shown in Table 5, LP(1)$N_{76} \rightarrow \sigma^*(C_{105}–H_{116})$ and LP(1)$N_{91} \rightarrow \sigma^*(C_{103}–H_{115})$ have the relatively larger stabilization energy $E^{(2)}$, 3.46 kcal/mol and 3.14 kcal/mol, respectively. The two orbital interactions signify the existence of the N–H···C hydrogen bonds, which provide an important contribution to the construction of the host–guest system. The $N_{76}–H_{116}···C_{105}$ hydrogen bond formed as the result of the orbital overlapping via the N_{76} atom donates lone pair electrons to the antibonding orbital of $C_{105}–H_{116}$. Similarly, the N_{91} atom donates lone pair electrons to the orbital of $C_{103}–H_{115}$ to form the $N_{76}–H_{116}···C_{105}$ hydrogen bond. Besides the traditional definition of hydrogen bonding, there also exists other weak interaction, for instance, the C–H···π bond which is relatively weaker than conventional hydrogen bonds in nature. The C–C bonding orbitals on the benzene ring can overlap with the C–H bonding orbitals of the MV^{2+} guest, which represents C–H···π hyper-conjugation. The C–H···π interaction is achieved by the delocalization of the π orbital. Its stabilization energies are relatively small, 1.10 kcal/mol and 0.94 kcal/mol, respectively. In addition, π–π stacking also affects the intermolecular interaction to a small extent. The orbital overlap between π(C–C) and π^*(C–C) results in intramolecular charge transfer, which conduces to improve the stability of the complexes. The stabilization energy $E^{(2)}$, which is found to be 0.98 kcal/mol, is affected by the intermolecular hyper-conjugative interaction between $\pi(C_{97}–C_{102})$ and antibonding orbital $\pi^*(C_{48}–C_{49})$. It is found that the hydrogen bonds play an essential role in stabilizing the conformation, and C–H···π interaction as well as π–π stacking also positively contributes to the stability of the system.

3.7 RDG analysis

To further illustrate the electron density characteristics of weak interactions in the complex, a visual approach called the reduced density gradient (RDG) is used to make it

Table 5 The electron donors, electron acceptors, and the corresponding second-order perturbation energy of the NBO analysis on orbital interactions

Donor NBO (i)	Acceptor NBO (j)	$E^{(2)}$ (kcal/mol)	$E_j - E_i$ (a. u.)	$F_{(i,j)}$ (a. u.)
BD(1)C97–H111	BD*(2)C18–C19	0.54	0.66	0.008
BD(2)C50–C51	BD*(2)C103–C108	0.31	0.25	0.008
BD*(2)C67–N76	BD*(1)C105–H116	1.10	0.78	0.027
LP(1)N75	BD*(1)C100–H113	1.33	0.79	0.030
LP(1)N76	BD*(1)C105–H116	3.46	0.80	0.048
LP(1)N91	BD*(2)C102–C114	0.45	0.79	0.017
LP(1)N91	BD*(1)C103–H115	3.14	0.80	0.046
BD*(2)C88–N91	BD*(1)C103–H115	0.94	0.78	0.025
BD*(1)C88–O93	RY*(1)H115	0.07	1.67	0.010
BD*(2)C97–C102	BD*(2)C48–C49	0.98	0.04	0.010

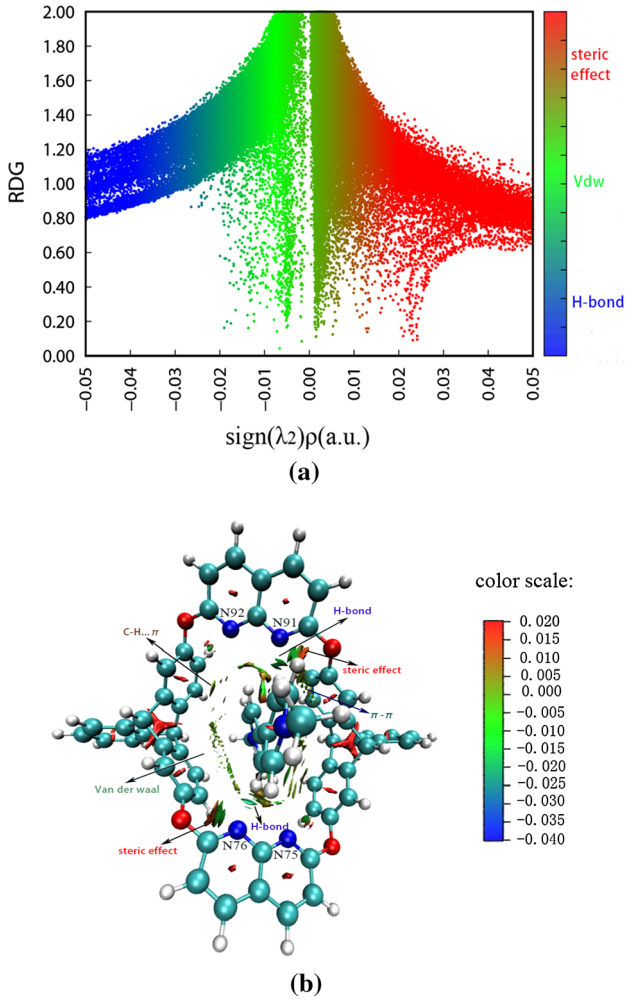

Fig. 6 The scatter diagram (**a**) and the gradient isosurfaces (**b**) for the MV^{2+}@TPA complex

more specific. The scatter diagram and the RDG isosurface map are shown in Fig. 6. The range of the function $\lambda 2(r)$ is defined between −0.04 and 0.02 a.u., the surface color is blue-green–red, and the area of $\lambda 2(r) < 0$ generally shows blue. As the blue becomes deeper, its attraction is stronger, generally including hydrogen bond, strong halogen bonds, and so on. The region of $\lambda 2(r) \approx 0$ displays green, which corresponds to the van der Waals (vdW) interaction. And the electron density here is small so that its sign is relatively unstable and could be positive or negative. The $\lambda 2(r) > 0$ region generally shows red, corresponding to the steric hindrance effect appearing in the ring and cage, and has strong mutual repulsion.

As shown in Fig. 6, two green–blue flaky regions near the N_{76} and N_{91} atoms, where oxygen and hydrogen atoms interact with each other, show a strong hydrogen bond, corresponding to the two hydrogen bonds of N_{76}–H_{116}···C_{105} and N_{91}–H_{115}···C_{103} analyzed in the previous NBO. It can be seen from the scatter plot that the peaks are located at the symbols $(\lambda 2)\rho \approx -0.020$ a.u. and −0.013 a.u. While other weak interactions such as C–H···π is showed by the brown-green flaky area in the Fig. 6(b). The $(\lambda 2)\rho$ value corresponding to the spike peak in the scatter plot is approximately −0.008 a.u.~ −0.002 a.u.n the cavity, a green area surrounds the guest molecule shown with broad green surfaces in the intermolecular spaces, indicating the van der Waals interaction between the complexes, corresponding to the −0.005 a.u. to 0.002 a.u. And region in the RDG scatter plot, with a red fusiform region in the middle of each benzene ring, reflects a strong steric effect, the corresponding spike on the right side of the scatter plot. (The scatter plot corresponds to a spike tip x value of approximately 0.012 a.u. and 0.024 a.u., respectively.) A small fragment of RDG isosurface between the C–H bonds of the triptycene benzene ring and the nitrogen atom of the naphthyridine is red and green and accounts for half of it, indicating that there is a steric effect. Thus, it can be concluded that the mutual exclusion and attraction effects coexist between the systems.

3.8 Topological analysis of electronic density (AIM)

The topological analysis has been used to further analyze the weak interactions between the molecules. In this theory, ρ, $\nabla^2\rho$, $G(r)$, $H(r)$, and $V(r)$ represent electron density, Laplacian of electron density, Lagrangian kinetic energy, energy density, and potential energy density, respectively, at the BCP along bond line (3, −1) for some interactions in this studied complex. Specifically, ρ is used to describe the strength of a bond, and the larger ρ value means a stronger bond. $\nabla^2\rho$ is used to characterize the bond strength, where a positive value often refers to ionic bonds, hydrogen bonds, or van der Waals interaction, while a negative $\nabla^2\rho$ value means the interatomic bond exists as covalent characteristic. And the positive value of $\nabla^2\rho$ also implies a closed-shell type interaction of a bond [44]. The requirement to satisfy the hydrogen bond is usually that the values of ρ are in the range from 0.002 to 0.040 a.u. and the values of $\nabla^2\rho$ are in the range of 0.024–0.139 a.u [45]. The AIM parameters for the weak interaction are listed in Table 6. The values of ρ and $\nabla^2\rho$ of I, II and III are all positive, which are in the range of 0.0080–0.0191 a.u. and 0.0261–0.0607 a.u., respectively. These values are within the acceptable H-bonds range, which ascertains the presence of C–H···N hydrogen bonding. This is consistent with the previous vibration frequency analysis. The C–H bond on the guest molecule vibrates toward the nitrogen atom in the host molecule, promoting the formation of C–H···N hydrogen bond. The value of ρ indicates that the N_{76}–H_{116}···C_{105} and N_{91}–H_{115}···C_{103} hydrogen bonds are stronger than N_{75}–H_{113}···C_{100} hydrogen bond. And the positive values of the energy density (H) indicate a dominant electrostatic contribution of these

Table 6 Selected AIM parameters (a.u.) for the weak interactions in the complexes

	Interaction	ρ (a.u.)	$\nabla^2\rho$ (a.u.)	G (a.u.)	V (a.u.)	H (a.u.)
I	N76–H116···C105	0.0191	0.0607	0.0130	−0.0107	0.0022
II	N91–H115···C103	0.0175	0.0550	0.0117	−0.0096	0.0021
III	N75–H113···C100	0.0080	0.0261	0.0047	−0.0039	0.0008
IV	C97–H111···π(C18–C19)	0.0069	0.0206	0.0042	−0.0032	0.0010
V	π(C97–C102)–π(C48–C49)	0.0051	0.0128	0.0026	−0.0020	0.0006

hydrogen bonds in the complex. It turns out that hydrogen bonds N_{76}–H_{116}···C_{105} and N_{91}–H_{115}···C_{103} play a more important role in this molecular system. It is also similar to the conclusions from the previous NBO analysis. According to the study of Rozas et al. [46], if $\nabla^2\rho > 0$ and $G + V > 0$, the intensity of the hydrogen bond is a weak hydrogen bond. In this work, the values of $\nabla^2\rho$ and $G + V$ were all positive, implying that the hydrogen bonds in the complex are weak. As for the IV and V, the ρ values are all within the scope of proposed criteria, while the $\nabla^2\rho$ values are beyond the lower limit of the range. They belong to C–H···π and π–π stacking interactions and play a certain role in stabilizing host and guest molecules.

4 Conclusions

A systematic analysis of the host–guest system between the triptycene-derived oxacalixarenes (TP) and paraquat derivatives has been carried out based on density functional theory. The DFT calculations were conducted to study the electronic and geometrical structure of these free species TPA, TPB, MV^{2+}, and their complexes. All the geometries structures were optimized using B3LYP-D3 and ωB97XD functionals with 6-311 + G(d, p) basis set. Based on the calculated results of interaction energy, it turned out that the complexation of *cis*-isomer TPA host and MV^{2+} guest is better than that of *trans*-isomer TPB host and MV^{2+} guest. Thermodynamic data signify that the inclusion reaction is spontaneous and exothermic. The MESP shows the electron-rich region is mainly localized on the nitrogen atoms of naphthalene ring, whereas the electron-deficient region is localized around the pyridine ring of the guest molecule. The changes in the ^{1}HNMR chemical shift indicate that the guest molecule is completely encapsulated within the host cavity. And the changes in vibration frequency shift verify the existence of weak intermolecular interactions. The host–guest system binding in such complexes is facilitated through hydrogen bonding, van der Waals, π···π stacking, as well as C–H···π interactions. Detailed analysis of molecular interaction through the NBO analysis combined with RDG and AIM methods enables distinguishing the attractive and repulsive interaction.

References

1. Lehn JM (1988) Supramolecular chemistry-scope and perspectives molecules, supermolecules, and molecular devices. Angew Chem Int Ed 27:89–112
2. Hoeben FJM, Jonkheijm P, Meijer EW (2005) About supramolecular assemblies of π-conjugated systems. Chem Rev 105:1491–1546
3. Cram DJ (1988) The design of molecular hosts, guests and their complexes. Angew Chem Int Ed 27:1009–1020
4. Steed JW, Turner DR, Wallace KJ (2007) Core concepts in supramolecular chemistry and nanochemistry. Wiley, West Sussex
5. Allwood BL, Spencer N, Shahriari-Zavareh H, Stoddart JF, Williams DJ (1987) Complexation of paraquat by a bisparaphenylene-34-Crown-10 derivative. J Chem Soc Chem Commun. https://doi.org/10.1039/C39870001064
6. Loeb SJ, Wisner JA (1998) A new motif for the self-assembly of [2]pseudorotaxanes; *1,2-bis*(pyridinium)ethane axles and [24] crown-8 ether wheels. Angew Chem Int Ed 37:2838–2840
7. Shen YX, Xie DH, Gibson HW (1994) Polyrotaxanes based on polyurethane backbones and crown ether cyclics. J Am Chem Soc 116:537–548
8. Odell B, Reddington MV, Slawin AMZ, Spencer N, Stoddart JF, Williams DJ (1988) Isostructural, alternately-charged receptor stacks the inclusion complexes of hydroquinone and catechol dimethyl ethers with cyclobis (paraquat-*p*-phenyiene). Angew Chem Int Ed 27:1547–1553
9. Ferguson SB, Sanford EM, Seward EM, Diederich F (1991) Cyclophane-arene inclusion complexation in protic solvents: solvent effects versus electron donor-acceptor interactions. J Am Chem Soc 113:5410–5419
10. Mason PE, Parsons IW, Tolley MS (1996) The first demonstration of molecular queuing in pseudo[N]polyrotaxanes: a novel variant of supramolecular motion. Angew Chem Int Ed 35:2238–2241
11. Harada A, Li J, Kamachi M (1992) The molecular necklace: a rotaxane containing many threaded a-cyclodextrins. Nature 356:325–327
12. Wenz G, Han BH, Müller A (2006) Cyclodextrin rotaxanes and polyrotaxanes. Chem Rev 106:782–817
13. Nepogodiev SA, Stoddart JF (1998) Cyclodextrin-based catenanes and rotaxanes. Chem Rev 98:1959–1976
14. Harada A, Takanishima Y, Yamaguchi H (2009) Cyclodextrin-based supramolecular polymers. Chem Soc Rev 38:875–882
15. Jiang J, Meng Y, Zhang L, Liu MH (2016) Self-assembled single-walled metal-helical nanotube (M-HN): creation of efficient supramolecular catalysts for asymmetric reaction. J Am Chem Soc 138:15629–15635
16. Mandl CP, König B (2004) Chemistry in motion unidirectional rotating molecular motors. Angew Chem Int Ed 43:1622–1624
17. Li C (2014) Pillararene-based supramolecular polymers: from molecular recognition to polymeric aggregates. Chem Commun 50:12420–12433
18. McKinlay RM, Atwood JL (2007) A hydrogen-bonded hexameric nanotoroidal assembly. Angew Chem Int Ed 119:2446–2449

19. Colasson B, Reinaud O (2008) Selective hetero-trisfunctionalization of the large rim of a biomimetic calix[6]arene using host-guest chemistry as a synthetic tool. J Am Chem Soc 130:15226–15227
20. Xue M, Chen C-F (2009) Triptycene-derived N(H)-bridged azacalixarenes: synthesis, structure, and encapsulation of small neutral molecules in the solid state. Org Lett 11:5294–5297
21. Xia Y-X, Xie T, Han Y, Chen C-F (2014) Triptycene-derived calix[6]arene analogues: synthesis, structure and complexation with paraquat derivatives. Org Chem Front 1:140–147
22. Yang J-S, Liu C-P, Lin B-C, Tu C-W, Lee G-H (2002) Solid-state molecular folding and supramolecular structures of triptycene-derived secondary dicarboxamides. J Org Chem 67:7343–7354
23. Tian X-H, Hao X, Liang T-L, Chen C-F (2009) Triptycene-derived calix[6]arenes: synthesis, structure and tubular assemblies in the solid state. Chem Commun 44:6771–6773
24. Zhang C, Chen C-F (2007) Triptycene-based expanded oxacalixarenes: synthesis, structure, and tubular assemblies in the solid state. J Org Chem 72:3880–3888
25. Hu S-Z, Chen C-F (2010) Triptycene-derived oxacalixarene with expanded cavity: synthesis, structure and its complexation with fullerenes C60 and C70. Chem Commun 46:4199–4201
26. Hu S-Z, Chen C-F (2011) Triptycene-derived oxacalixarenes as new wheels for the synthesis of [2]rotaxanes: acid–base- and metal-ion-switchable complexation processes. Chem Eur J 17:5424–5431
27. Johnson ER, Keinan S, Mori-Sánchez P, Contreras-Garcia J, Cohen AJ, Yang W (2010) Revealing noncovalent interactions. J Am Chem Soc 132:6498–6506
28. Frisch MJ, Trucks GW, Schlegel HB, Scuseria GE, Robb MA, Cheeseman JR, Scalmani G, Barone V, Mennucci B, Petersson GA, Nakatsuji H, Caricato M, Li X, Hratchian HP, Izmaylov AF, Bloino J, Zheng G, Sonnenberg JL, Hada M, Ehara M, Toyota K, Fukuda R, Hasegawa J, Ishida M, Nakajima T, Honda Y, Kitao O, Nakai H, Vreven T, Montgomery JA Jr, Peralta JE, Ogliaro F, Bearpark M, Heyd JJ, Brothers E, Kudin KN, Staroverov VN, Kobayashi R, Normand J, Raghavachari K, Rendell A, Burant JC, Iyengar SS, Tomasi J, Cossi M, Rega N, Millam JM, Klene M, Knox JE, Cross JB, Bakken V, Adamo C, Jaramillo J, Gomperts R, Stratmann RE, Yazyev O, Austin AJ, Cammi R, Pomelli C, Ochterski JW, Martin RL, Morokuma K, Zakrzewski VG, Voth GA, Salvador P, Dannenberg JJ, Dapprich S, Daniels AD, Farkas O, Foresman JB, Ortiz JV, Cioslowski J, Fox DJ (2013) Gaussian 09, versions D.01. Gaussian, Inc., Wallingford
29. Chai J-D, Head-Gordon M (2008) Long-range corrected hybrid density functionals with damped atom–atom dispersion corrections. Phys Chem Chem Phys 10:6615–6620
30. Grimme S, Antony J, Ehrlich S, Krieg H (2010) A consistent and accurate ab initio parametrization of density functional dispersion correction (DFT-D) for the 94 elements H-Pu. J Chem Phys 132:154104–154119
31. Goerigk L, Grimme S (2011) A thorough benchmark of density functional methods for general main group thermochemistry, kinetics, and noncovalent interactions. Phys Chem Chem Phys 13:6670–6688
32. Tomasi J, Mennucci B, Cammi R (2005) Quantum mechanical continuum solvation models. Chem Rev 105:2999–3094
33. Roy DD, Todd AK, John MM (2009) Gauss View 5.0.8. Gaussian, Inc., Wallingford
34. Politzer P, Murray JS, Clark T (2015) Mathematical modeling and physical reality in noncovalent interactions. J Mol Model 21:52
35. Wolinski K, Hinton JF, Pulay P (1990) Efficient implementation of the gauge-independent atomic orbital method for NMR chemical shift calculations. J Am Chem Soc 112:8251–8260
36. Baldridge KK, Siegel JS (1999) Correlation of empirical Δ(TMS) and absolute NMR chemical shifts predicted by ab initio computations. J Phys Chem A 103:4038–4042
37. Barone V, Cossi M, Tomasi J (1998) Geometry optimization of molecular structures in solution by the polarizable continuum model. J Comput Chem 19:404–417
38. Boys SF, Bernardi F (1970) The calculation of small molecular interactions by the differences of separate total energies. Some procedures with reduced errors. Mol Phys 19:553–566
39. Reed AE, Curtiss LA, Weinhold F (1988) Intermolecular interactions from a natural bond orbital, donor–acceptor viewpoint. Chem Rev 88:899–926
40. Humphrey W, Dalke A, Schulten K (1996) VMD: visual molecular dynamics. J Mol Graph 14:33–38
41. Bader RFW (1990) Atoms in molecules: a quantum theory. Oxford University Press, Oxford
42. Lu T, Chen F (2012) Quantitative analysis of molecular surface based on improved marching tetrahedra algorithm. J Mol Graph Model 38:314–323
43. Lu T, Chen F (2012) Multiwfn: a multifunctional wavefunction analyzer. J Comput Chem 33:580–592
44. Roohi H, Nowroozi AR, Anjomshoa E (2011) H-bonded complexes of uracil with parent nitrosamine: a quantum chemical study. Comput Theor Chem 965:211–220
45. Koch U, Popelier PLA (1995) Characterization of C–H–O hydrogen bond on the basis of the charge density. J Phys Chem 99:9747–9754
46. Rozas I, Alkorta I, Elguero J (2000) Behavior of ylides containing N, O, and C atoms as hydrogen bond acceptors. J Am Chem Soc 122:11154–11161